Nanoscale

Accepted Manuscript

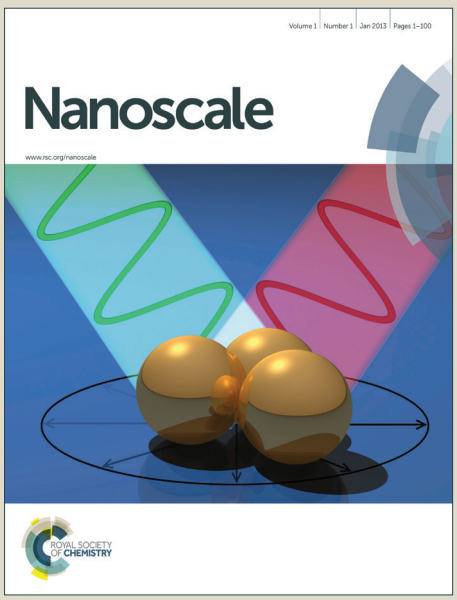

ROYAL SOCIETY OF CHEMISTRY

www.rsc.org/nanoscale

Revised manuscript submit to ***Nanoscale***

Manuscript ID: **Nanoscale - NR-ART-07-2015-004971**

High energy output nanogenerator based on reduced graphene oxide

Weiping Li,[a,b]‡ Yupeng Zhang,[a,c]‡ Liangliang Liu,[a]‡ Delong Li,[a,b] Lei Liao,[a] Chunxu Pan[a,b]*

[a] *School of Physics and Technology, and MOE Key Laboratory of Artificial Micro- and Nano-structures, Wuhan University, Wuhan, Hubei 430072, China.*

[b] *Shenzhen Research Institute, Wuhan University, Shenzhen, Guangdong 518057, China.*

[c] *Department of Materials Science & Engineering, Monash University, Clayton, Victoria 3800, Australia.*

* Corresponding author.
E-mail address: cxpan@whu.edu.cn (C. Pan)

‡ These authors contributed equally to this work.

Abstract

In this paper, we report a novel graphene-based nanogenerator for high energy harvesting. Experimental and theoretical results revealed that the energy output mechanism was the joint action of the strain effect (band engineering) and triboelectric effect of reduced graphene oxide. It was found that the current could be adjusted by experiment parameters, such as electrolyte concentration and rotation rate. Furthermore, the voltage output could be amplified by series connect of the system. Compared with other nanogenerators, the present graphene-based nanogenerator provides advantages, such as simple assembly, flexibility and high structural stability. It is expected this nanogenerator is of potential applications in active sensors and sustainable power source.

Introduction

The past few decades has witnessed a great number of breakthroughs in nano- science and technology. Many of the practical electronic, photonic and optoelectronic devices have achieved success in various applications, which includes the batteries, transistors, nanogenerator and so on.[1-3] As the energy harvested from the nature environment becomes a growing portion of sustainable energy source, the nanogenerator which collect the nano-energy have established their importance in this active and emerging field.[4-6]

Basically, a high efficient nanogenerator is based on two critical points: electrode materials and physical effect during power generation. Recently, the well-known nanogenerators are based on two physical effects: the piezoelectric effect [7] and triboelectric effect.[8] The piezoelectric nanogenerator can be described as a transient flow of electrons driven by the piezopotential. When the nanogenerator is subject to a compressive stress, a piezopotential field is created. As a result, inductive charges accumulate on the top and bottom electrodes. The most commonly used electrodes materials for the piezoelectric nanogenerator includes ZnO, CdS, GaN, PZT (Piezoelectric Ceramic Transducer), PVDF (Polyvinylidene Fluoride), etc.[9-11] The triboelectric nanogenerator converts mechanical energy into electricity using the coupling effects between triboelectrification and electrostatic induction through the contact-separation between two materials that have opposite tribo-polarity. PMMA (Polymethyl Methacrylate)-Kapton, Au-PDMS (Polydimethylsiloxane), Ag-PTFE (Polytetrafluoroethylene), Al-PDMS, etc. are used as electrode system for the triboelectric nanogenerator. [12-14]

Recently, graphene has attracted significant scientific interest, due to its outstanding mechanical, electrical and thermal properties,[15-17] and been considered as a promising material for the next generation electronics. S. Kim, et. al. [18] successfully demonstrated the application of CVD-grown graphene as the transparent, flexible triboelectric nanogenerators (TNGs).

Graphene-based TNGs (GTNGs) based on monolayer, bilayer, trilayer, and quad-layer graphene, and few-layer graphene grown on Cu and Ni foils using CVD have been fabricated, and their output voltage and output current density were measured under mechanical strains. The monolayer-GTNG exhibited a highoutput voltage and output current density of 5 V and 500 nA·cm^{-2}, respectively. Theoretical calculations and experimental results have demonstrated that the strain in graphene lattice can dramatically modify its band structure and electrical properties.[19-21] Our previous work has found that the chemical potential could be generated from a mechanically strained monolayer graphene sheet, which provides an alternative way to fabricate a graphene-based device.[22]

In this paper, we report a graphene (reduced graphene oxide, RGO) based nanogenerator for harvesting mechanical energy through joint action of the strain effect (band engineering) and triboelectric effect. Our experimental design originates from the idea that the micro-strain and friction can be applied on the graphene sheets by stirring the electrolyte on the surface of graphene, and then electric output is generated in an electrochemical system.

Results

Fig. 1a illustrated the RGO based energy harvesting system, which capable of converting mechanical energy into electricity by band engineering effect of RGO. SEM observation revealed that the RGO electrode consisted of well exfoliated and dispersive graphene sheets on a nickel foam substrate (Fig. 1b). In the electrochemical system, the energy (voltage and current) was obviously produced according to the stirring of the electrolyte, as shown in Fig. 1c. A series of control experiments and corresponding results were provided to support the validity of the method and the authenticity of the data (Supplementary Information, Fig. S1).

Here, we propose two effects for joint action upon this energy harvesting, that is, the strain (band engineering) effect of graphene sheets and triboelectric effect between graphene and electrolyte.

In order to verify the strain effect, two different graphene sheets, i.e., RGO from chemical exfoliation [23] and graphene from chemical vapor deposition (CVD), named C-graphene, were used as the electrode materials, respectively. The experimental results revealed that the electric output could be generated from RGO, instead of C-graphene, as shown in Fig. 2a. In general, it is known that there are a lot of oxygenic functional groups and defects on the RGO surface,[24] while there is a clear surface for C-graphene.[25] Integrated Raman intensity mapping of the D band (1250-1500 cm^{-1}) of RGO revealed that the functional groups were uniformly distributed on the electrode materials (Fig. 2b). XPS and FTIR spectrum showed that the some chemical functional groups such as hydroxyl (C-OH), carboxyl (C=O, O=C-OH), and epoxide group (C-O-C) could be introduced on the RGO surface (Supplementary Information, Fig. S2). Therefore, when the electrolyte was stirred slowly in the system, the oxygenic functional groups on the RGO surface vibrated. This phenomenon can be explained as a result of the friction force between RGO and the electrolyte, which induced a strain effect in RGO sheets and tuned the band gap of RGO. Then, the band gap variation changed the RGO electrochemical properties involving chemical potential, adsorption and ion transportation. The electric output was generated in the electrochemical system subsequently.

We also presented the integration of experimental setup in a microfluidic system, and used Raman spectroscopy to characterize the structure changes of RGO sheets in microfluidic system, which could further help us to verify the strain effect (Supplementary Information, Fig. S3). When fluid (Na_2SO_4 solution) flows along the channel on the RGO sheets, the Raman spectra of RGO changed weakly. The results revealed that the full width at half maximum (FWHM) of D and G band had the broad trend, and the value of I_D / I_G ratio

changed from 0.76 to 0.88. The change of Raman spectra could indicate the structural variation of RGO, which provide evidence that the strain effect was achieved by friction between RGO sheet and electrolyte.

Theoretical calculations were carried out in order to understand the above experimental results (Fig. 3 and Supplementary Information, Fig. S4).[26-28] The friction force between the electrolyte and RGO could disturb oxygenic functional groups from their equilibrium sites, and caused the graphene vibration in its inherent frequencies. The results revealed that the band-gap opened about 160 meV wide and the C-OH group plays the most important role, when the RGO sheet whose atoms shifted along one of vibration (Fig. 3b), which gave a good explanation for the above experimental results.

In addition to the above strain effect, the triboelectric effect between RGO sheets and electrolyte could also convert the mechanical energy into electrical energy. Fig. 4 gives the parameters which exhibited strong influences on the energy output. From the *i-t* curve in Fig. 4a, the triboelectric effect and strain effect could be clearly distinguished, because that the former brought out a pulsed current, whereas the latter produced a steady-state current. Furthermore, the triboelectric effect could also be verified by changing the concentration of the electrolyte (Na_2SO_4 solution). The experimental results indicated that with increasing the electrolyte concentration, the triboelectric effect between graphene and electrolyte strengthened gradually, which resulted in the increasing of the current density, as shown in Fig. 4b. It was confirmed that the electrolyte concentration played a key role in increasing the energy output (current). Similarly, the rotation rate of the electrolyte also greatly influenced energy output, as shown in Fig. 4c and 4d. In addition, during the experiment for mouths, it have been found that the sample was of a long cycle life without decay, and we believe that the RGO-based nanogenerator has a favorable stability.

Besides the current, voltage is also an important target for the nanogenerator. However, due to the existing of oxygenic functional groups and defects, the conductivity of RGO is

poor, and the RGO-based electrode exhibits a large contact resistance. This means that the voltage of RGO-based nanogenerator cannot be improved greatly by adjusting the parameters. In order to analyze the mechanism of electrochemical process and to evaluate the kinetics of the RGO/Ni electrode, electrochemical impedance spectra (EIS) was measured and an equivalent circuit was used to simulate the EIS data. Fig. S5 (Supplementary Information) showed the Nyquist plots of RGO/Ni electrode in 1 M Na_2SO_4 at 0.1V. The equivalent circuit included elements, such as, bulk solution resistance (R_{sol}), pseudocapacitance (CPE_1, low) and double-layer capacitance (CPE_2, high) due to RGO, and charge transfer resistance (R_{ct}). When the electrolyte was stirred, the induced current flowed through the circuit to the collector electrode. However, a voltage drop would occur across each resistance, which resulted in the output voltage not be improved greatly. Therefore, we used a series connection for the voltage amplification. The results showed that the voltage could be duplicated when two nanogenerators were connected, as shown in Fig. 5 and Fig. S6 (Supplementary Information).

Discussion

We elucidate the mechanism of the nanogenerator based on RGO as follows: Since the existing of oxygenic functional groups and defects, RGO should be negatively charged.[29, 30] In the electrolyte, an excessive cloud of counter-ions named as the electrical double layer is formed adjacent to the negatively charged RGO electrode. In this case, the intrinsic potential difference will be generated between the RGO working electrode and the counter electrode. When RGO is strained mechanically, the band structure of RGO will be tuned obviously, which will further contribute to the change of the absorption, conductivity and the electrochemical properties such as electrical double layer capacitor of RGO. As an inevitable sequence result, an intrinsic potential difference significantly changes between the working and counter electrodes, which can be realized by the separation and transport of ionic charges

in the electrolyte. Finally, in the electrochemical system, the ionic flow is transformed into a steady-state current in the process of straining RGO.

On the other hand, the pulsed current is attributed to the separation and transport of the local charges on the graphene surface. At first, we assumed that the stirring velocity and the friction between each electrode and the electrolyte were constant according to the experiments. Since the RGO surface contained the polarized groups, an excessive cloud of counter-ions was formed (almost on the oxygenic functional groups and defects) adjacent to the negatively charged RGO sheets. When the electrolyte was stirred, ions in the electrolyte would interact with the cloud of ions on the RGO sheets, which resulted in a net ionic flow (the cloud of ions moved from the sites of oxygenic functional groups and defects to the sheet surfaces). The ionic flow needed to be balanced by the electric current. Therefore, the pulsed current generated (Supplementary Information, Fig. S7).

When we improved the rotating speed of electrolyte, the interactions of ions were intensified, and the pressure on the RGO sheets was increased due to stirring, which led to an acceleration of ionic flow. The pulsed current became larger subsequently. Meanwhile, when we improved the electrolyte concentration, the number of ions per unit volume was increased, which resulted in an enhancement of the ions interactions. The pulsed current became larger similarly.

The above experimental and calculation results demonstrates the energy harvesting from the RGO based nanogenerator due to the joint action of the strain effect and triboelectric effect of RGO. This explanation has provided wide prospects for the application of RGO nanogenerator. For instance, we have measured the seawater power generator by using the RGO nanogenerator when we changed the electrolyte into seawater (Supplementary Information, Fig. S8). Surprisingly, the results revealed that the power output per unit area could improve by five times due to the high concentration and variety of ions in seawater.

In summary, for the RGO nanogenerator, the current output can be adjusted by parameters, such as electrolyte concentration and rotation rate. And the voltage output can be amplified from series connection. Comparing to other nanogenerators, the graphene-based nanogenerator provides advantages such simple assembly, flexibility and high structural stability. This nanogenerator is expected to have potential applications in active sensors and sustainable power source.

Methods

Graphene oxide (GO) was synthesized from natural graphite by a modified Hummers method. The product was purified by dialysis to completely remove residual salts and acids, and then calcined at 700 ℃ for 2 hours under argon atmosphere with a heating rate 100 ℃/min. At last, RGO sheets were obtained.

The surface morphology of RGO was examined by SEM (FEI SIRION, Netherland) operated at 15 kV. Chemical compositions and chemical environment of the carbon atoms on the RGO were measured by using Raman spectroscopy (HORIBA Jobin Yvon LabRAM HR, France).

The electrical output of RGO under the friction of electrolyte was measured by using an electrochemical workstation (CHI660C, Chenhua, China). An Ag/AgCl electrode was used as a reference electrode, which was filled with 3 M NaCl (BASi). A piece of RGO/nickel foam (1 cm × 2 cm) and a platinum plate were used as the working electrode and counter electrode, respectively. The working and counter electrode were attached on a plastic plate (PTFE plate) to avoid the vibration of the electrode when the electrolyte was stirred. Meanwhile, the distance between working and counter electrode was fixed at 3 cm. Na_2SO_4 solutions (0-2 M) were used as the electrolyte. For the measurement of electrical output, an external force was applied to make the electrolyte keep in stirring, which produced a friction force between RGO

sheets and the electrolyte, and resulted in electrical output in the electrochemical system. The output voltage and current were recorded by a open circuit potential test and the amperometric *i-t* curve test, respectively.

Density functional theory (DFT) calculations were used to study the band structure of graphene. The calculations were performed using a Vienna Ab-initio Simulation Pack-age (VASP). The valence electronic states were expanded in a set of periodic plane waves and the interaction between core electrons and the valence electrons was implemented through the projector augmented wave (PAW) approach. The Perdew-Burke-Ernzerhof (PBE) GGA exchange-correlation functional was applied in the calculations, In relaxation, summations over the Brillouin zone (BZ) were performed with a 4 × 4 × 1 Monkhorst Pack k-point mesh. The smooth part of the wave functions was expanded in plane waves with a kinetic energy cutoff of 400 eV and the convergence criteria for the electronic and ionic relaxation were 10^{-4} eV and 0.02 eV/Å, respectively. An orthorhombic 12.329 Å × 12.812 Å (60 atoms) supercell was used in the computation, and the calculated C-C bond length was 1.425 Å in the perfect graphene. One C vacancy and four Hydroxyl groups (OH) were induced in the graphene to simulate the defects. The vacuum layer with a thickness of 15 Å on the graphene surface was big enough to reduce the interaction between two pieces of graphene.

Acknowledgements

This work was supported by the National Nature Science Foundation of China (No. 11174227), Special Fund for the Development of Strategic Emerging Industries of Shenzhen City of China (No. JCYJ20140419141154246), and National Key Technology R&D Program of Hubei province of China (No. 2013BHE012).

Additional information

Supplementary Information:

Competing financial interests: The authors declare no competing financial interests.

References

1 X. Chen, C. Li, M. Grätzel, R. Kostecki, S. S. Mao, *Chem. Soc. Rev.*, 2012, **41**, 7909-7937.

2 Q. Bao, H. Zhang, B. Wang, Z. Ni, C. H. Y. X. Lim, Y. Wang, D. Y. Tang, K. P. Loh, *Nature photon.*, 2011, **5**, 411-415.

3 L. Liao, Y. C. Lin, M. Bao, R. Cheng, J. Bai, Y. Liu, Y. Qu, K. L. Wang, Y. Huang, X. F. Duan, *Nature*, 2010, **467**, 305-308.

4 Z. L. Wang, G. Zhu, Y. Yang, S. Wang, C. Pan, *Mater. Today*, 2012, **15**, 532-543.

5 R. A. Whiter, V. Narayan, S. K. Narayan, *Adv. Energy Mater.*, 2014, **4**, 1400519.

6 Y. Mao, P. Zhao, G. McConohy, H. Yang, Y. Tong, X. Wang, *Adv. Energy Mater.*, 2014, **4**, 1301624.

7 X. Wang, J. Song, J. Liu, Z. L. Wang, *Science*, 2007, **316**, 102-105.

8 F. R. Fan, R. Lin, G. Zhu, W. Wu, R. Zhang, Z. L. Wang, *Nano Lett.*, 2012, **12**, 3109-3114.

9 C. T. Huang, J. Song, W. F. Lee, Y. Ding, Z. Gao, Y. Hao, L. J. Chen, Z. L. Wang, *J. Am. Chem. Soc.*, 2010, **132**, 4766-4771.

10 X. Chen, S. Xu, N. Yao, Y. Shi, *Nano Lett.*, 2010, **10**, 2133- 2137.

11 S. Bae, O. Kahya, B, K. Sharma, J. Kwon, H. J. Cho, B. Ozyilmaz, J. H. Ahn, *ACS nano*, 2013, **7**, 3130-3138.

12 F. Fana, Z. Tian, Z. L. Wang, *Nano Energy*, 2012, **1**, 328-334.

13 J. Chen, G. Zhu, W. Yang, Q. Jing, P. Bai, Y. Yang, T. C. Hou, Z. L. Wang, *Adv. Mater.*, 2013, **25**, 6094- 6099.

14 X. S. Zhang, M. D. Han, R. X. Wang, F. Y. Zhu, Z. H. Li, W. Wang, H. X. Zhang, *Nano Lett.*, 2013, **13**, 1168-1172.

15 K. S. Novoselov, A. K. Geim, S. V. Morozov, D. Jiang, Y. Zhang, S. V. Dubonos, I. V. Grigorieva, A. A. Firsov, *Science*, 2004, **306**, 666-669.

16 K. S. Novoselov, D. Jiang, Y. Zhang, S. V. Morozov, H. L. Stormer, U. Zeitler, J. C. Maan, G. S. Boebinger, P. Kim, A. K. Geim, *Science*, 2007, **315**, 1379.

17 T. J. Booth, P. Blake, R. R. Nair, D. Jiang, E. W. Hill, U. Bangert, A. Bleloch, M. Gass, K. S. Novoselov, A. K. Geim, *Nano Lett.*, 2008, **8**, 2442-2246.

18 S. Kim, M. K. Gupta, K. Y. Lee, A. Sohn, T. Y. Kim, K. Shin, D. Kim, S. K. Kim, K. H. Lee, H. Shin, D. Kim, S. Kim, *Advanced Materials*, 2014, **26**, 3918-3925.

19 C. P. Chang, B. R. Wu, R. B. Chen, M. F. Lin, *J. Appl. Phys.*, 2007, **101**, 063506.

20 Z. H. Ni, T. Yu, Y. H. Lu, Y. Y. Wang, Y. P. Feng, Z. X. Shen, *ACS Nano*, 2008, **2**, 2301-2305.

21 M. Huang, T. A. Pascal, H. Kim, W. A. Goddard, J. R. Greer, *Nano Lett.*, 2011, **11**, 1241-1246.

22 Y. Zhang, C. Luo, W. Li, C. Pan, *Nanoscale*, 2013, **5**, 2616-2619.

23 Y. Zhang, D. Li, X. Tan, B. Zhang, X. Ruan, H. Liu, C. Pan, L. Liao, T. Zhai, Y. Bando, S. Chen, W. Cai, R. S. Ruoff, *Carbon*, 2013, **54**, 143-148.

24 S. Stankovich, R. D. Piner, X. Chen, N. Wu, S. T. Nguyen, R. S. Ruoff, *J. Mater. Chem.*, 2006, **16**, 155-158.

25 X. Li, W. Cai, J. An, S. Kim, J. Nah, D. Yang, R. Piner, A. Velamakanni, I. Jung, E. Tutuc, S. K. Banerjee, L. Colombo, R. S. Ruoff, *Science*, 2009, **324**, 1312-1314.

26 P. E. Blöchl, *Phys. Rev. B*, 1994, **50**, 17953-17979.

27 G. Kresse, D. Joubert, *Phys. Rev. B*, 1999, **59**, 1758-1775.

28 G. Kresse, J. Hafner, *Phys. Rev. B*, 1993, **48**, 13115-13118.

29 P. Dhiman, F. Yavari, X. Mi, H. Gullapalli, Y. Shi, P. M. Ajayan, N. Koratkar, *Nano Lett.*, 2011, **11**, 3123- 3127.

30 D. Li, M. B. Muller, S. Gilje, R. B. Kaner, G. G. Wallace, *Nature nanotech.*, 2008, **3**, 101-105.

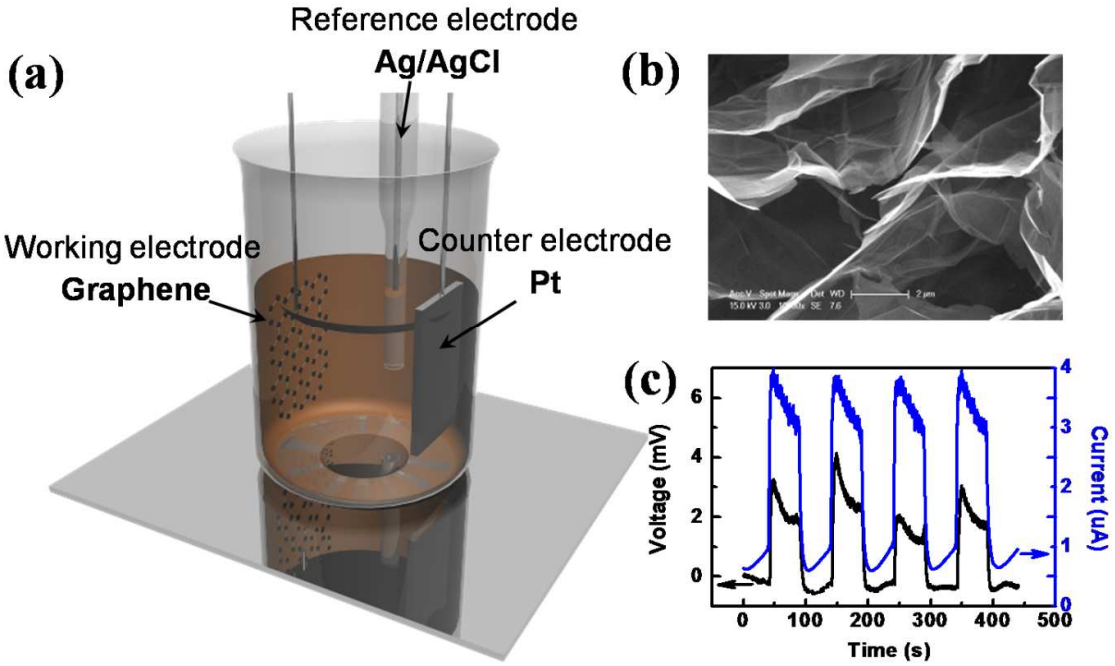

Fig. 1 RGO based energy harvesting system. (a) Schematic model of the system; (b) SEM image of the RGO/Ni foam electrode; (c) Voltage and current profiles obtained from the RGO in the electrolyte that been slowly stirred.

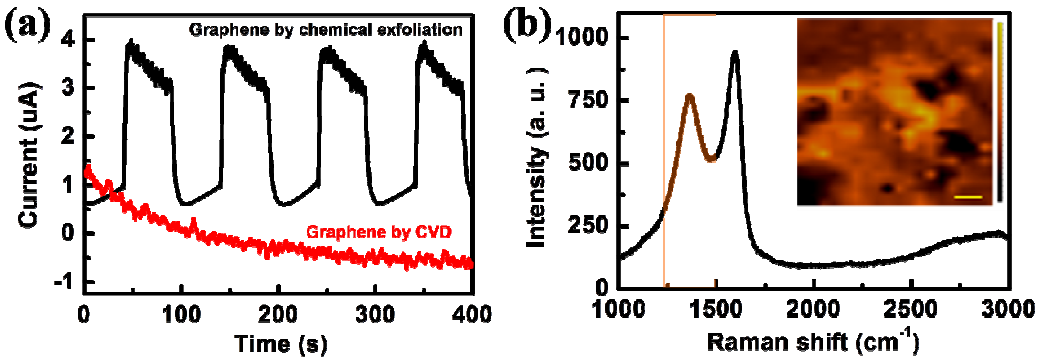

Fig. 2 (a) Current obtained from RGO and C-graphene in electrolyte that been slowly stirred. (b) Raman characterization of RGO, inset in (b) is a Raman image of the D-band intensity, the scale bar is 5 μm.

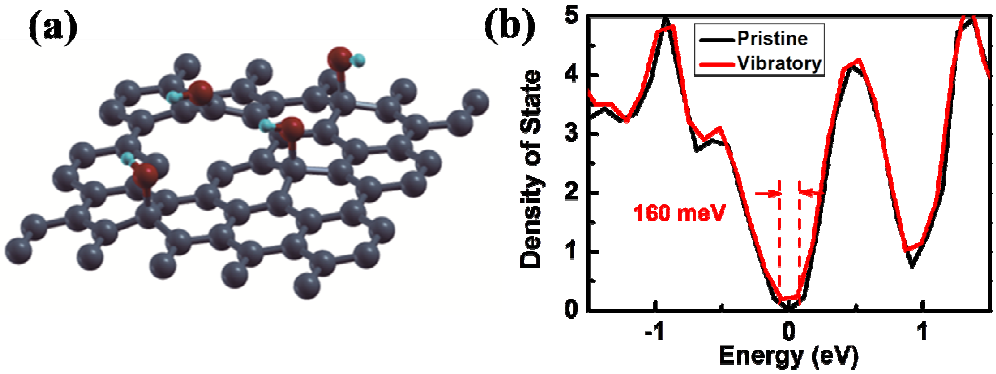

Fig. 3 Theoretical calculations of RGO sheet under different states. (a) Structural model; (b) Density of states of pristine and the vibratory sheets.

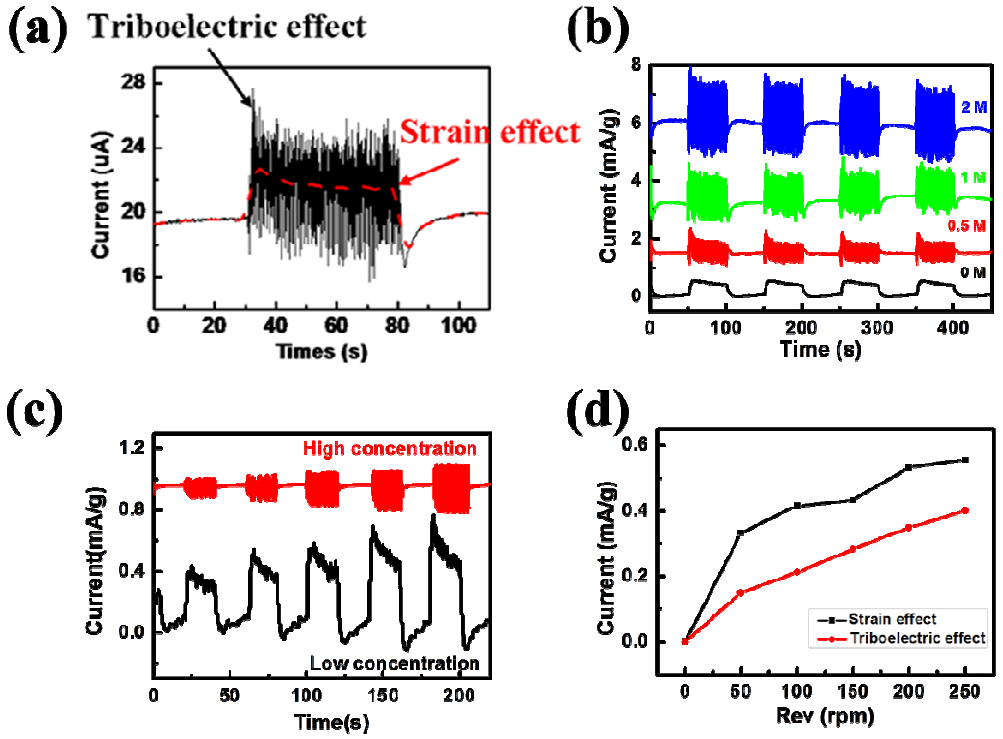

Fig. 4 Relationships between current output and parameters. (a) Triboelectric effect; (b) Electrolyte concentrations; (c) and (d) Rotation rate of electrolyte.

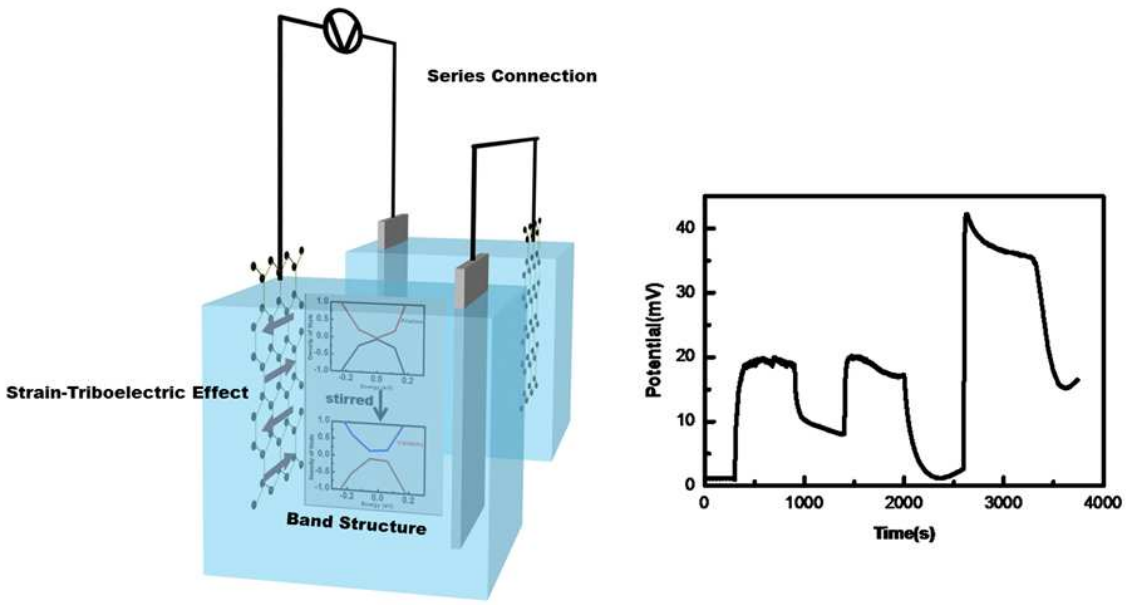

Fig. 5 Voltage amplification of nanogenerator by series connection.